Influence of Fuel Properties on Gasoline Direct Injection Particulate Matter Emissions Over First 200 s of World-Harmonized Light-Duty Test Procedure Using an Engine Dynamometer and Novel "Virtual Drivetrain" Software

Noah R. Bock
Department of Mechanical Engineering,
University of Minnesota,
Minneapolis, MN 55455
e-mail: bockx081@umn.edu

William F. Northrop[1]
Department of Mechanical Engineering,
University of Minnesota,
Minneapolis, MN 55455
e-mail: wnorthro@umn.edu

The influence of fuel properties on particulate matter (PM) emissions from a catalytic gasoline particulate filter (GPF) equipped gasoline direct injection (GDI) engine was investigated using novel "virtual drivetrain" software and an engine mated to an engine dynamometer. The virtual drivetrain software was developed in LABVIEW to operate the engine on an engine dynamometer as if it were in a vehicle undergoing a driving cycle. The software uses a physics-based approach to determine vehicle acceleration and speed based on engine load and a programed "shift" schedule to control engine speed. The software uses a control algorithm to modulate engine load and braking to match a calculated vehicle speed with the prescribed speed trace of the driving cycle of choice. The first 200 s of the World-harmonized Light-duty Test Procedure (WLTP) driving cycle was tested using six different fuel formulations of varying volatility, aromaticity, and ethanol concentration. The first 200 s of the WLTP was chosen as the test condition because it is the most problematic section of the driving cycle for controlling PM emissions due to the cold start and cold drive off. It was found that there was a strong correlation between aromaticity of the fuel and the engine-out PM emissions, with the highest emitting fuel producing more than double the mass emissions of the low PM production fuel. However, the post-GPF PM emissions depended greatly on the soot loading state of the GPF. The fuel with the highest engine-out PM emissions produced comparable post-GPF emissions to the lowest PM producing fuel over the driving cycle when the GPF was loaded over three cycles with the respective fuels. These results demonstrate the importance of GPF loading state when aftertreatment systems are used for PM reduction. It also shows that GPF control may be more important than fuel properties, and that regulatory compliance for PM can be achieved with proper GPF control calibration irrespective of fuel type. [DOI: 10.1115/1.4050576]

Keywords: gasoline particulate filter, gasoline direct injection, World-harmonized Light-duty Test Procedure, fuel properties, particulate matter, air emissions from fossil fuel combustion, fuel combustion

Introduction

Mitigating the emission of harmful pollutants and greenhouse gasses remains a challenge in the development of internal combustion engines and vehicle systems as regulatory standards continue to become increasingly stringent [1,2]. The use of gasoline direct injection (GDI) engines has been widely adopted, with the majority of new light-duty vehicles powered by GDI engines [3]. GDI engines can attain higher thermal efficiency than their port fuel injection (PFI) counterparts; however, particulate matter (PM) emissions are a persistent concern with GDI engines due to the nature of the fuel delivery method to the combustion chamber [4–6]. PM emission control is primarily achieved through a combination of engine control strategies, exhaust aftertreatement devices, and fuel formulation [7]. These three aspects must be analyzed from both a component level approach and a system-level approach to understand their impact on PM emissions and opportunities for synergistic reduction of PM emissions.

High particulate matter emissions from GDI engines relative to PFI engines are due to the reduced charge mixing time after the start of injection. This leads to charge inhomogeneity as well as cylinder wall and piston surface wetting. Fuel-rich regions in the cylinder undergo incomplete combustion and pyrolysis of the fuel which causes soot formation [7–9]. Fuel formulation also plays an important role in soot formation. This includes both thermodynamic properties, such as heat of vaporization (HoV), energy density, and volatility, and chemical properties, such as aromaticity. Lower volatility fuels require higher temperatures and longer times

[1]Corresponding author.

Contributed by the Internal Combustion Engine Division of ASME for publication in the JOURNAL OF ENERGY RESOURCES TECHNOLOGY. Manuscript received February 22, 2021; final manuscript received March 8, 2021; published online April 19, 2021. Editor: Hameed Metghalchi.

to evaporate, which leads to charge inhomogeneity and soot formation [10]. Partial oxidation of aromatic compounds is known to produce soot precursors, thus, fuels with high concentrations of aromatics generally produce higher PM emissions [11]. Fuel oxygenates have varying effects on soot formation, depending on concentration and oxygenate. Ethanol, for example, has been shown to increase soot concentrations under some conditions and reduce soot concentrations under others [12–15]. This is due to two counteracting effects: higher concentrations of ethanol diluted the concentration of aromatics in the fuel, reducing soot; however, the high heat of vaporization of ethanol inhibits the evaporation of the fuel, leading to poor charge composition [16].

Fuel properties can be analyzed to determine a fuel's propensity for PM emissions. A predictive model for calculating a fuel's propensity for PM production, called the PM Index, was developed by Aikawa et al. [17]. The PM Index is based on the mass fraction, double bond equivalent (DBE), and vapor pressure of each of the fuel's components. The equation for calculating the PM Index is shown in Eq. (1)

$$\text{PM Index} = \sum_{i=1}^{n}\left(\frac{\text{DBE}_i + 1}{P_{vap,i}(443\text{ K})} \times Wt_i\right) \tag{1}$$

where DBE_i is the double bond equivalent for component i, $P_{vap,i}$ (443 K) is the vapor pressure of component i at 443 K, and Wt_i is the weight fraction of component i. Aikawa et al. showed a good correlation between the PM Index and PM emissions operating over the New European Driving Cycle (NEDC).

Gasoline particulate filters (GPFs) have been shown to significantly reduce the tailpipe emissions of PM over regulatory driving cycles. Particle number (PN) and PM reductions range between 60% and more than 90%, depending on a number of factors including filter porosity, filter pore size, catalyst loading, soot loading, driving cycle, and other vehicle parameters [18]. As soot is loaded on the GPF, the filter pores fill with soot, which increases the filtration efficiency. However, this also increases the pressure drop across the filter. The filter must be regenerated by oxidizing the soot once the pressure drop becomes high enough to affect fuel efficiency. Ideally, a soot loading level could be maintained that optimized both filtration efficiency and fuel efficiency. Implementation of GPFs in GDI engine-equipped vehicles is becoming prevalent in Europe to meet Euro 6c PN limits, in China to meet China 6(b) PN limits in 2020 [19], and may be introduced in the United States to as stricter LEV III PM standards are phased in.

Driving cycle testing is conducted with a vehicle on a chassis dynamometer, also known as a rolling dyno, with the vehicle following a prescribed speed trace of a regulatory driving cycle that approximates real-world driving. Emissions and fuel consumption are measured over the cycle to determine compliance. Thus, determining if a vehicle meets regulatory compliance requires a fully assembled vehicle. Because engine testing and calibration early in the development process is conducted on an engine dynamometer, testing driving cycles with an engine dynamometer could reduce the time required for in-vehicle calibration on a chassis dynamometer and in real-world tests. Testing driving cycles on an engine dynamometer would allow engine control strategies and aftertreatment components to be modified before final vehicle assembly.

Testing driving cycles with an engine dynamometer requires a model of drivetrain components and vehicle specifications in order to operate the engine as if it was in a vehicle performing in the vehicle itself on the road. The literature review yielded few published works on testing driving cycles using an engine dynamometer. Keder et al. proposed an engine dynamometer test stand for driving cycle simulation [20]. The authors outlined all necessary hardware and software, including a vehicle model, which would allow the operation of an engine on an engine dynamometer as though it was operating in a vehicle performing a driving cycle. However, no experimental engine data were presented, so it is not known whether the system was successful at completing its objectives. In a master's thesis by Androne and Rao, a hardware-in-loop methodology was applied to an engine dynamometer and vehicle model to operate and engine over the World-harmonized Light-duty Test Procedure (WLTP) and NEDC driving cycles [21]. They were able to control the engine to match calculated vehicle speed within 2 km/h of the driving cycle speed traces and showed comparable fuel consumption and CO_2 emissions to the engine in a vehicle running the driving cycles on a chassis dynamometer.

No previous published work was found on PM emissions from an engine on an engine dynamometer operating over a driving cycle. In the current study, the authors sought to determine the impact of fuel properties on engine-out and post-GPF PM emissions of a GDI engine operating overcritical portions of a relevant driving cycle.

Methods/Experimental. The test engine used in this study was a BMW N43B20 2.0 L, naturally aspirated, in-line four-cylinder engine. The engine specifications are listed in Table 1. This engine was used in BMW 120i, 320i, and 520i vehicles in the European market from model years 2007–2011. The engine featured centrally mounted, outward opening, spray guided piezoelectric injectors. The engine was controlled by a National Instruments Powertrain Controls engine controller in lieu of the factory engine controller to allow full control of all engine parameters. The calibration was developed by another research group and National Instruments at Oak Ridge National Laboratory using a vehicle on a chassis dynamometer with the factory engine controller [15]. A three-way catalyst (TWC) wash-coated GPF was installed in the exhaust of the engine to evaluate filtration performance.

A virtual drivetrain model was designed in LABVIEW software to control the dynamometer in such a way that the engine would behave as if it were connected to a transmission in a vehicle. A schematic/flowchart of the virtual drivetrain, the driving cycle controller, and the engine hardware is shown in Fig. 1. The virtual drivetrain inputs were brake torque, engine speed, virtual gear "vGear," virtual brake "vBrake," and vehicle specifications to calculate an instantaneous acceleration. The drivetrain model loop was executed with a specified Δt value of 100 ms. Then, the calculated acceleration is multiplied by Δt to calculate the change in vehicle speed over the time-step, which is added to the previously calculated vehicle speed, to obtain the new calculated vehicle speed. To determine vehicle acceleration, the net road force is calculated using Eq. (2)

$$F_{road} = F_{driveline} + F_d + F_{rr} + F_{brake} \tag{2}$$

where F_{road} is the net road force, $F_{driveline}$ is the driveline force produced by the engine, F_d is the aerodynamic drag force, F_{rr} is the rolling resistance, and F_{brake} is the braking force. The driveline force produced by the engine is the product of the brake (crank) torque, the current gear ratio, the final drive ratio, the driveline efficiency, and the inverse of tire radius. The calculation for the driveline force is calculated using Eq. (3)

$$F_{driveline} = \tau_{crank} R_g R_{fd} \eta_{driveline} r_{tire}^{-1} \tag{3}$$

where τ_{crank} is the crank torque produced by the engine, R_g is the gear ratio of the current gear, R_{fd} is the final drive ratio, $\eta_{driveline}$

Table 1 Test engine geometry and specifications

Model number	N43B20
Displacement (cc)	1995
Bore × Stroke (mm)	84 × 90
Compression ratio	12:1
Rated power (kW)	125 @ 6700 rpm
Rated torque (Nm)	210 @ 4250 rpm
Induction	Naturally Aspirated
Injection	Central Spray Guided Piezo Injectors
Max rail pressure (bar)	200

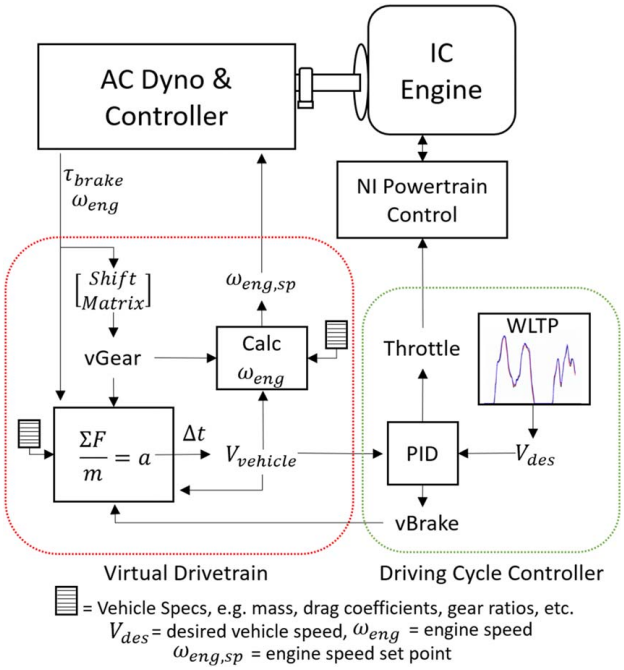

Fig. 1 Schematic of virtual drivetrain, driving cycle controller, and engine hardware

is the driveline efficiency, and r_{tire} is the tire radius. The aerodynamic drag force is calculated using Eq. (4)

$$F_d = -\frac{1}{2} C_d \rho V_{vehicle}^2 A_f \tag{4}$$

where C_d is the drag coefficient of the vehicle, ρ is the air density, $V_{vehicle}$ is the vehicle velocity, and A_f is the frontal area of the vehicle. The rolling resistance force is calculated as the product of the coefficient of friction for the tires and road C_f, the mass of the vehicle m, and the acceleration due to gravity g. The equation for the rolling resistance force is shown in Eq. (5)

$$F_{rr} = -C_f mg \tag{5}$$

The vehicle acceleration was calculated as the ratio of the road force over the mass of the vehicle. The equation for vehicle acceleration, $a_{vehicle}$, is shown in Eq. (6)

$$a_{vehicle} = \frac{F_{road}}{m} \tag{6}$$

The vehicle velocity was calculated by adding the previous vehicle velocity, $V_{vehicle,o}$, to the product of the vehicle acceleration and loop execution time, Δt, and is shown in Eq. (7)

$$V_{vehicle} = V_{vehicle,o} + a_{vehicle} \Delta t \tag{7}$$

A set of shift matrices within the virtual drivetrain controlled what virtual gear (vGear) the vehicle was in. The shift matrix inputs were engine speed and load, then it was determined if an "upshift" or "downshift" was required based on engine speed and percent load. There were unique shift matrices for gears 1, 2, and 3–6. The virtual brake (vBrake) was a variable in the virtual drivetrain model representing a braking force from 0 to 10 kN. When the vBrake was be applied, the total road force became negative, which decreased the calculated vehicle speed, and thus the engine speed until a downshift was determined to be required. The driving cycle controller was a proportional–integral–differential (PID) controller that took calculated vehicle speed and desired vehicle speed as inputs and output a signal to the throttle or the vBrake to either increase or decrease the vehicle speed. The set of described components allowed the engine to operate over any predefined vehicle speed trace as if it were in a vehicle performing the speed trace.

Seven different fuel formulations were tested in the experimental study. A list of fuels and fuel properties is shown in Table 2 including percentage of aromatics, distillation temperature T90, ethanol concentration, ani-knock index (AKI) where AKI is the arithmetic mean of the research octane number (RON) and the motor octane number (MON), and PM Index. The fuels were formulated based on a baseline E10 Euro 6 certification fuel. They were match blended to change one fuel property while keeping the others as close to the baseline as possible.

The emissions sampling system and measurement instrumentation are shown in Fig. 2. As described in previous work [16], gaseous emissions were measured using an AVL (Graz, Austria) SESAM i60 FT multi component exhaust measurement system composed of a Fourier transform-infrared (FT-IR) spectrometer, a flame ionization detector (FID), and a paramagnetic oxygen detector. PM emissions were measured by an AVL MicroSoot Sensor (MSS), two TSI (Shoreview, MN) engine exhaust particle sizers (EEPSs), and two TSI condensation particle counters (CPCs) with 11 nm cutoff sizes. The MSS measured soot mass concentration upstream of the GPF, the EEPSs simultaneously measured particle size distributions (PSDs) upstream and downstream of the GPF at a rate of 1 Hz using the soot inversion matrix to determine real-time, size-resolved GPF filtration efficiency, and the CPCs measured PN concentration pre- and post-GPF. Two catalytic strippers (CSs) were operated at 300 °C in order to remove all volatile and semi-volatile material from the exhaust gas such that the particle emissions measured by EEPSs and CPCs were that of only solid particles. The CS operating principles and performance are described in other work [22].

Table 2 Fuel properties tested

Fuel ID	Aromatics (%)	T90 (°C)	EtOH (%)	AKI	PMI
Baseline	27.0	162	9.9	90.8	NA
A-1	**22.4**	160	9.9	90.9	1.2
A-2	**42.9**	166	9.9	92.6	1.8
V-1	29.4	**129**	9.9	90.8	0.7
V-2	29.4	**187**	10.0	91.7	2.2
E15	28.5	160	**15.2**	93.6	1.4
E50	16.7	160	**50.0**	96.3	1.1

Note: Bold values indicates that these are the properties deviated from the baseline fuel.

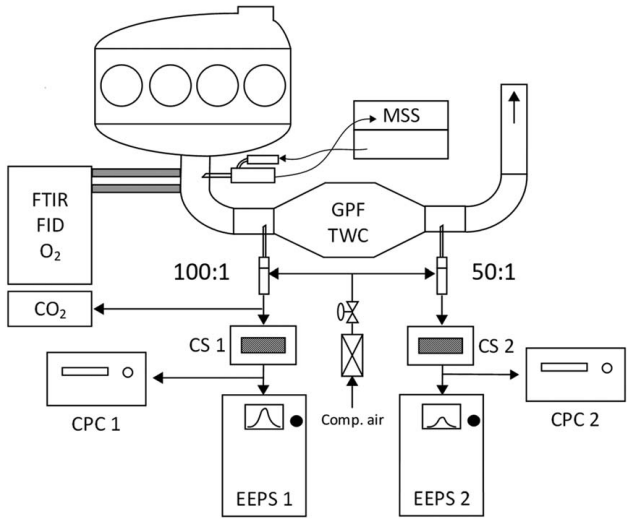

Fig. 2 Engine and instrumentation schematic showing dilution system and instruments used in the experimental study

Exhaust sample for particle measurement required dilution to "freeze" the size distributions by decreasing the particle concentration to inhibit the particle coagulation rate so that the PSDs did not shift to larger sizes. Dilution was also required to reduce the water concentration to eliminate condensation as well as to keep the particle concentrations within the measurement limits of the particle instruments. Ejector pump (EP) diluters were used with critical orifices to maintain a constant sample flowrate. The pre-GPF dilution ratio was approximately 100 ± 1:1 and was measured throughout testing using the CO_2 concentration measured downstream of the diluter by an infrared CO_2 detector. The post-GPF dilution ratio was approximately 50 ± 1:1 and was measured by the same method as the pre-GPF dilution ratio, but it was measured prior to testing as opposed to during testing. Particle loss through the CS was characterized in a previous study, and all reported particle emissions in this study are loss corrected by the method described in that work [23]. Particle mass was calculated from the particle size distributions measured by the EEPS and the size-dependent density function determined by Maricq and Xu for a GDI vehicle operating under steady-state conditions [24].

The first 200 s of the WLTP cycle was selected for evaluating PM emissions. This portion of the driving cycle is the most problematic for PM emissions due to cold start and cold drive off. Each fuel was tested under this portion of the driving cycle three times. The GPF was regenerated before each fuel was tested, so each fuel test started with a clean filter. The GPF loaded over the course of three runs for a specific fuel before it was regenerated for testing the next fuel. GPF regeneration was accomplished by running ~700 °C exhaust through the filter under slightly lean conditions for 10 min followed by a fuel cut. The engine was cold soaked after each test such that all engine components were at ambient temperature (~20 °C) before starting the next test. The fuel system and engine were purged and flushed with new fuel prior to starting the testing the next fuel test.

Results and Discussion

Vehicle driving cycle data were provided by an automotive partner for a vehicle with a similar displacement, naturally aspirated engine operating over the WLTP cycle on a chassis dynamometer. Vehicle speed traces are shown in Fig. 3 for the target speed of the WLTP, the simulated vehicle speed using the virtual drivetrain and engine dynamometer, and for a medium-sized vehicle on the chassis dynamometer. The maximum deviation from the speed trace for the engine dynamometer was less than 1 mph, and the average deviation over the test was less than 0.1 mph. This was true for every fuel and was extremely repeatable due to the nature of the virtual drivetrain (maximum deviations in same location and of same magnitude), thus only the trace for the baseline fuel on the engine dyno is shown.

Figure 4 shows the test engine torque and speed compared with the engine in the vehicle over the first 200 s of the WLTP cycle. The speed and torque traces of the BMW test engine were comparable to that of the actual vehicle. The torque output for the chassis dynamometer vehicle is a calculated crank torque from an ECU lookup table, which is likely why there are large spikes at throttle tip-in. However, the trends in torque are very similar between the chassis dynamometer and the engine dynamometer. The toque discrepancy at idle is due to torque converter drag and ancillary loads not associated with the engine dyno. The trends in engine speed for the engine dynamometer and chassis dynamometer also are in good agreement. The slight differences in torque and engine speed between the engine dynamometer test and the chassis dynamometer test can be attributed to differences in shift matrices. The shift matrix for the engine dynamometer tended to hold gears longer than the chassis dyno, resulting in slightly higher engine speed and lower brake torque for some portions of the cycle to attain the same acceleration.

Average PSDs are shown for the pre-GPF and post-GPF sampling location in Fig. 5. These are average size distributions emitted for each fuel over three runs of the first 200 s of the WLTP. The standard deviation for each curve is approximately one order of magnitude due to spikes and dips in concertation due to fuel tip-in and fuel cut and is not shown, so the individual curves can be clearly seen. The E50 fuel produced the lowest average particle concentrations of any fuel throughout the size range. Under these conditions, the dilution of aromatics was

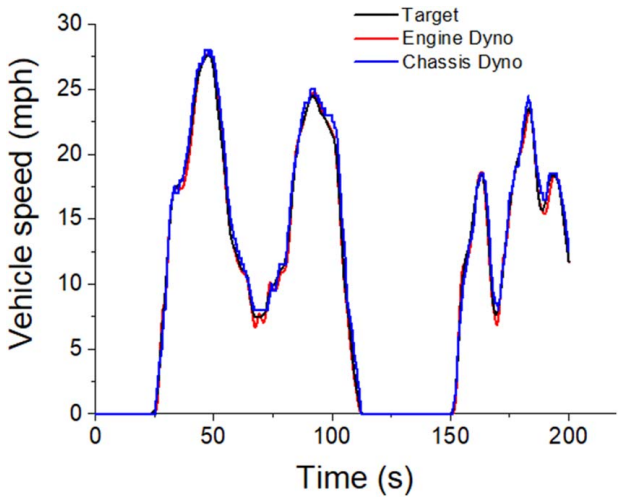

Fig. 3 Simulated vehicle speed versus time over the first 200 s of the WLTP cycle compared with the manufacturer-provided data and the prescribed target speed for the cycle

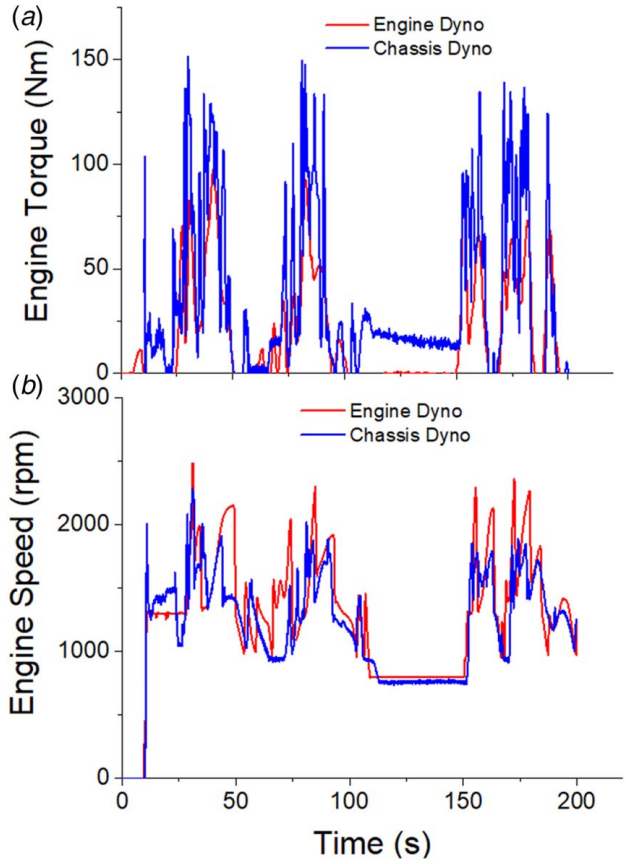

Fig. 4 (*a*) Engine torque and (*b*) engine speed versus time over the first 200 s of the WLTP cycle compared with the manufacturer provided

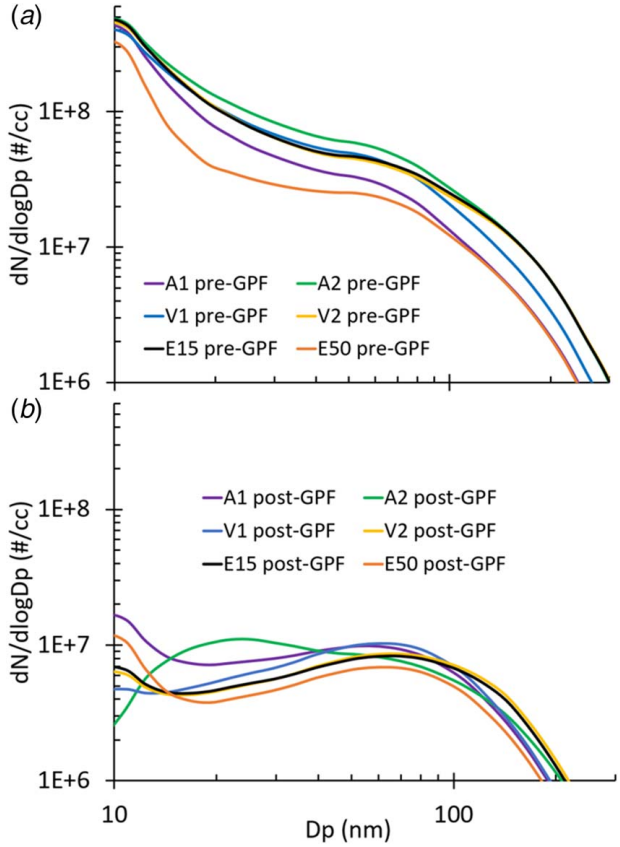

Fig. 5 (*a*) Average pre-GPF and (*b*) post-GPF PSDS over the first 200 s of the WLTP

dominant, outweighing the effect of delayed fuel evaporation caused by the high HoV of the ethanol. The high aromatics fuel produced the highest average particle concentrations of any fuel throughout the entire size range. It appears under these conditions the pathway from aromatics to soot precursors is dominant in producing PM compared with the volatility effect because the low volatility fuel has the highest PM Index but produced fewer particles on average.

All fuels produced large 10 nm ash modes thought to originate from lubrication oil additives. This is consistent with the observed high oil consumption of the engine. The peaks of the ash mode generally followed the trend of the ~80 nm accumulation (soot) mode. If the accumulation and ash mode formation mechanisms were independent from one another, it would be expected that the ash mode would decrease as the accumulation mode increased due to the large soot particles scavenging the small ash particles. However, because this is not the case, it appears that the ash and soot mode are linked. As discussed in previous work, there may be fuel impingement on the cylinder walls which partially washes away the oil film and allows it to detach, atomize, and eventually be burned, leaving behind only the noncombustible ash particles [16].

The post-GPF size distributions show the GPF was very effective at removing the 10 nm ash mode. The concentration of 10 nm ash particles was reduced by two orders of magnitude for most fuels, corresponding to a filtration efficiency of 99% at this size. However, because such a large ash mode was emitted from the engine-out location, a significant amount of 10 nm ash particles slipped through the GPF. Current PN emission limits are for particles greater than 23 nm under the European Particle Measurement Programme (PMP) [25]. Due to the high toxicity of very small particles, it is possible that the PN regulatory limits will be reduced to include 10 nm particles in the future. Because many GPFs can capture more than 99% of 10 nm particles, they may not be thought to a concern with GPF implementation. However, with a clean GPF and high oil consumption, these results show that there can be considerable 10 nm particle penetration. This could be addressed by optimizing filter pore size for >99% filtration efficiency with a clean filter. On the other hand, an engine with very high ash emissions will eventually load the filter with ash and increase the filtration efficiency, mitigating the ash slip problem.

Figures 6 and 7 show the pre- and post-GPF solid PN > 23 nm and PM emissions calculated from EEPS PSDs for three fuels over three runs with error bars representing one standard deviation. The fuels highlighted here are the highest emitter (the high aromatics fuel A-2), the lowest emitter (E50), and one in between the two (the low volatility fuel V-1).

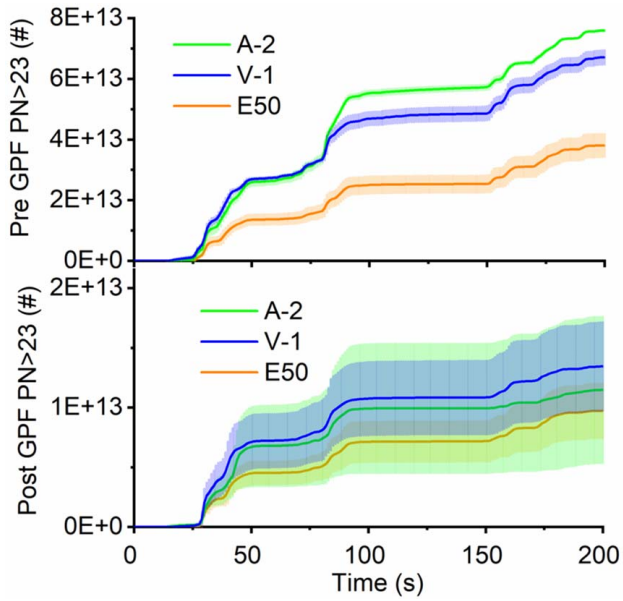

Fig. 6 Cumulative solid PN > 23 nm pre- and post-GPF over the first 200 s of the WLTP

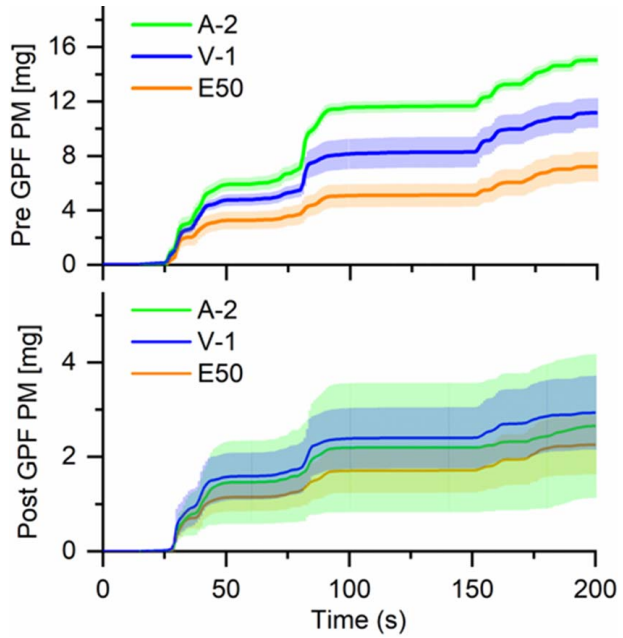

Fig. 7 Cumulative PM pre- and post-GPF over the first 200 s of the WLTP

The pre-GPF emissions were very repeatable with each fuel showing distinct traces. For the first 200 s of the WLTP cycle, the high aromatics fuel produced the highest cumulative pre-GPF emissions and the high ethanol fuel producing the lowest cumulative pre-GPF emissions. However, there was high run-to-run variability in the post-GPF emissions. The highest variability was seen for the A-2 fuel. The A-2 fuel had the highest post-GPF emissions of the three fuels on the first run with a clean GPF; however, the A-2 fuel had the lowest post-GPF PM emissions of any fuel on the third run. The high engine-out PM emissions from the A-2 fuel loaded the GPF over the first two runs and increased its filtration efficiency to a high level. Even though the engine-out emissions stayed high during the third run, because the GPF filtration efficiency was sufficiently high, the post-GPF emissions were lower than any fuel. This shows the significance of the state of loading of the GPF. The E50 fuel produced the lowest average cumulative post-GPF PM emissions. However, the A-2 fuel produced the second-lowest average cumulative post-GPF PM emissions, even though the average pre-GPF emissions were much high than the V-1 fuel.

The effect of the soot loading on GPF filtration efficiency over the three runs is shown in Fig. 8. Again, fuels A-2, V-1, and E50 are highlighted to show the trends with a high, mid, and low emitting fuel, respectively. For each fuel, the filtration efficiency curve increased for each subsequent run as soot was loaded over the three runs. For each fuel, the most penetrating particle size (MPPS) was near 100 nm and for each run (ignoring downward slopes around 500 nm for now), and for each fuel, the filtration efficiency at MPPS on the first run was just under 60%. This shows each round of fuel testing started with a clean filter. For the A-2 fuel, the filtration efficiency exceeded 90% at 100 nm on the third run, whereas the V-1 fuel and E50 fuel only reached 77% and 67%, respectively, at 100 nm on their third runs. The total filtration efficiency for PN > 23 is shown in the legend. By the third run the E50 fuel only reaches 0.784, while the A-2 fuel reaches 0.928. This illustrates how the highest engine-out emitting fuel, A-2, produced lower post-GPF emissions than the lowest engine-out emitting fuel, E50.

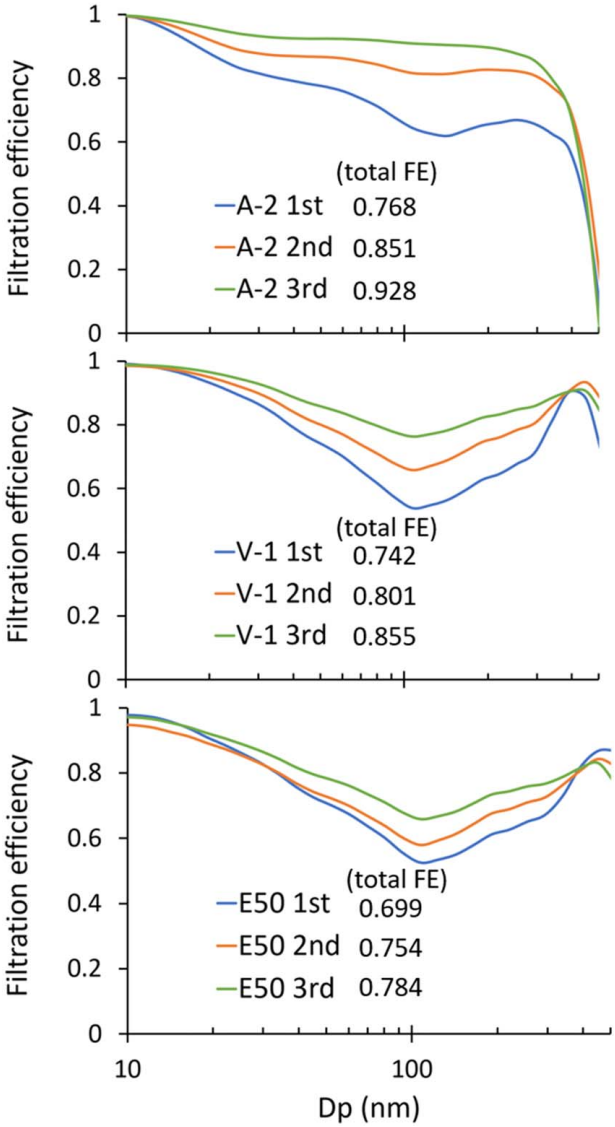

Fig. 8 Average size-resolved filtration efficiency over each 200 s run of the WLTP for fuels A-2, V-1, and E50 with total filtration efficiency for PN > 23 nm listed for each run

The filtration efficiency curves all showed an unusual drop in filtration efficiency near 500 nm. This is unusual because for most filter media, the MPPS is near 100–200 nm. Particles smaller than the MPPS are effectively trapped by diffusion, and particles larger than that are effectively trapped by impaction and interception [26]. From examining the time resolved PSD data for each run, there are very few ~500 nm particles emitted from the engine-out location. However, at around 180 s elapsed time into the cycle, there was a large spike in ~500 nm particles from the post-GPF location for all fuels, with no emission of particles of this size at the pre-GPF location. During this period, the engine goes from a high load to a fuel-cut condition.

Initially, the post-GPF spike in PM was thought to maybe a partial regeneration. However, the GPF temperature only got as high as ~150 °C, which is too low for regeneration. It is currently unclear what caused this throughout all the tests. Particles of this size could be catalyst material from the GPF releasing during a sudden change in filter flowrate; suspended soot particles of this size are very rare. Another explanation could be the release of coagulated soot particles at the back of the filter. This would be an interesting area to explore, but because the relative concentration of the ~500 nm particles is orders of magnitude less than particles in the 10–100 nm size range, the tail in the filtration efficiency curve does not significantly affect the total filtration efficiency. Furthermore, these 500 nm particles do not significantly contribute to the overall number or mass of particles emitted.

Comparisons between cumulative soot mass emitted and cumulative PN > 23 nm emitted over the first 200 s of the WLTP cycle with the PM Index and fuel aromatics concentration at the engine-out location are shown in Fig. 9. The soot concentration measured by the MSS correlated about equally well with the aromatics concentration as it did with the PM Index, with an *r*-squared value of ~0.5. The engine-out PN > 23 correlated well with the aromatic concentration of the fuel, but poorly with the PM Index. This may be explained by looking at the soot and PN > 23 nm concentrations. There should be a strong linear correlation between soot mass and PN > 23 nm if particle density and the particle size distribution remain constant.

A discrepancy can be seen between the PN > 23 and soot concentration in the order of the relative magnitudes for each fuel. The low volatility fuel, V-2, produced the highest soot concentrations but the high aromatics fuel, A-2, produced the highest PN > 23 nm concentrations. From examining the particle size distributions in Fig. 5, the A-2 fuel emitted a higher fraction of particles between 23 nm and 100 nm than the V-2 fuel. Above 100 nm, the PSDs from the two fuels converge. If the soot mass emitted was equal for the A-2 and V-2 fuels, it could be explained that most of the particle mass is in the distribution above 100 nm. However, because the V-2 has higher soot mass than A-2, it would seem to indicate that it also has higher soot density.

Figure 10 shows correlations between post-GPF PM emissions and the fuel aromatics concentration and PM Index. No correlation existed between the post-GPF PM emissions and aromatics or the PM Index. The post-GPF PM emissions were not significantly

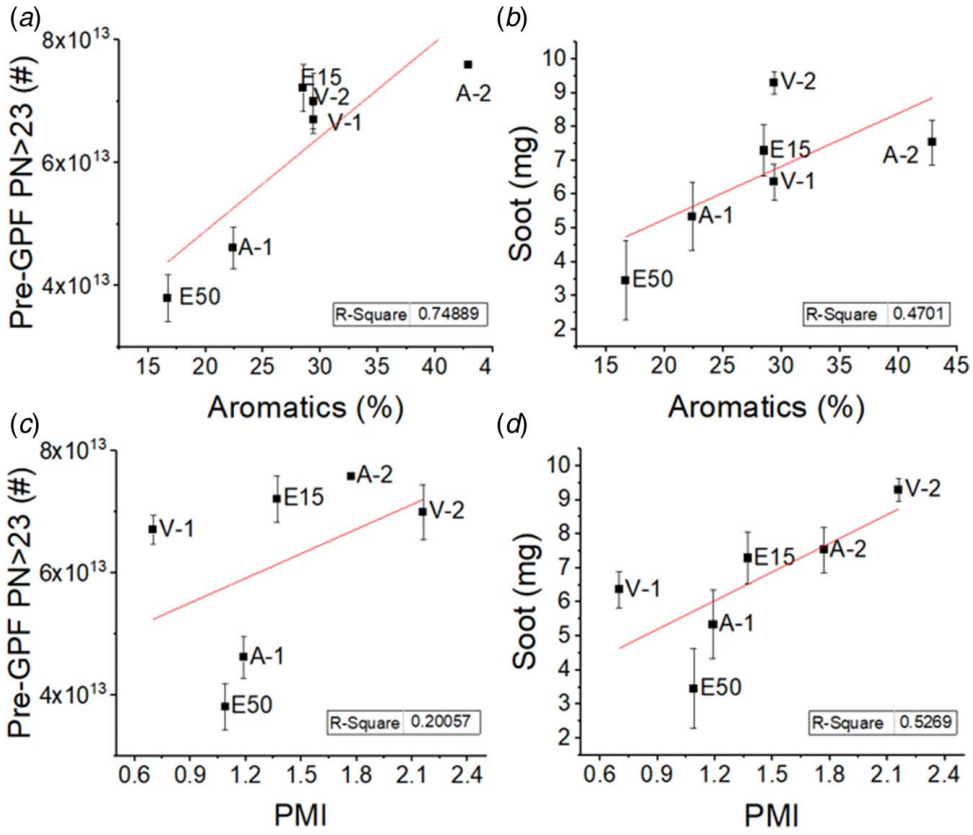

Fig. 9 Correlation between (*a*) cumulatve pre-GPF PN > 23 nm and aromatics, (*b*) pre-GPF soot and aromatics, (c) pre-GPF PN > 23 nm and PMI, and (*d*) pre-GPF soot and PMI

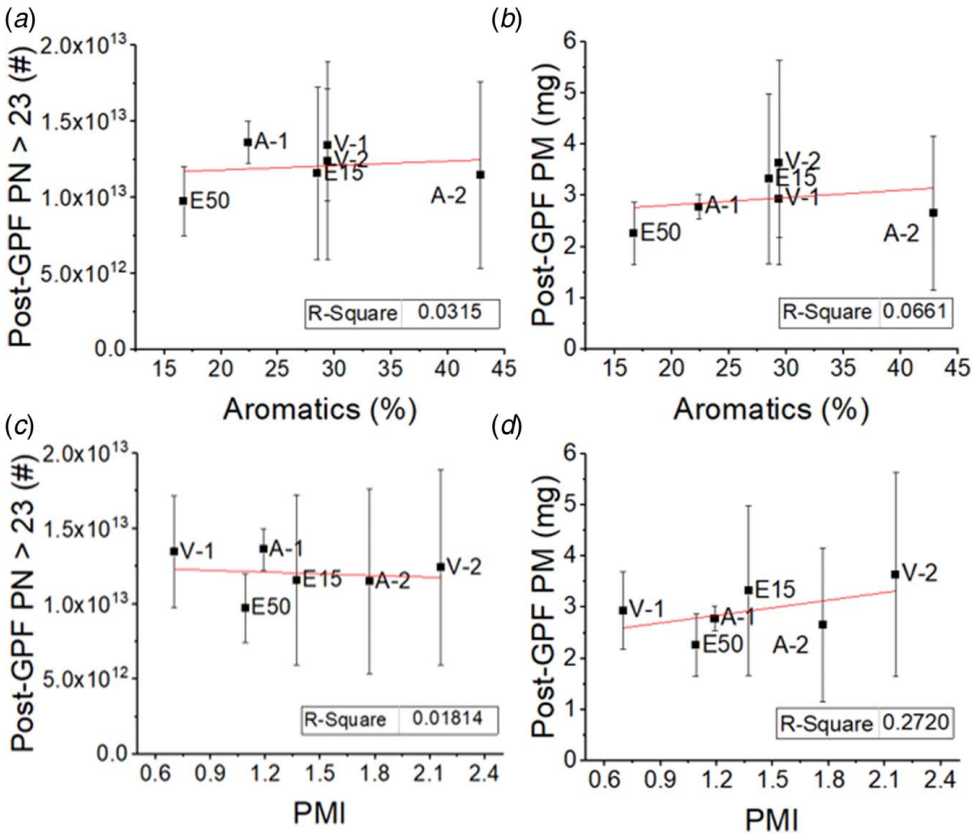

Fig. 10 Correlation between (*a*) cumulatve post-GPF PN > 23 nm and aromatics, (*b*) post-GPF PM and aromatics, (c) post-GPF PN > 23 nm and PMI, and (*d*) post-GPF PM and PMI

different from each other. This was due to, as discussed earlier, the GPF loading faster for the fuels the emitted higher engine-out PM. The first 200 s of the WLTP corresponds to 0.93 km of distance traveled, so the cumulative emissions shown are approximately the same as the emission per km, e.g., mg/km. If only looking at the first 200 s, all of the fuels would fail the Euro 6c PN limit of 6×10^{11} part./km for this section of the test and all would pass the Euro 6c and PM limit of 4.5 mg/km with the GPF installed. Though the PN number limit is much harder to achieve, and as the engine warms up over the cycle, the lower emissions through the remainder of the cycle may be enough to bring the average #/km emissions below the limit. Future work will seek to evaluate this over the entire driving cycle.

Conclusions

Driving cycle testing was demonstrated with an engine on an engine dynamometer using a novel, software programmed virtual drivetrain. The virtual drivetrain commanded the engine to operate under speed and load conditions as if it were performing the driving cycle. Calculated vehicle speed was well within the acceptable limits of the driving cycle, and engine speed and load traces were comparable to that of a similarly sized engine running the driving cycle on a chassis dynamometer. This development allowed PM emission testing and GPF performance evaluation over a driving cycle with the use of an engine dynamometer. The virtual drivetrain offers an option for testing driving cycles without the expense and footprint of a vehicle on a chassis dynamometer. This expands the limits for what can be done at certain research facilities and can reduce engine calibration and emission control development time in corporate engineering departments.

Particulate matter emissions were measured pre- and post-GPF with six different fuel formulations over the first 200 s of the WLTP cycle. The results showed high PM emissions from all fuels and illustrated why this challenging section of the regulatory cycle is important for mitigating emissions. Each fuel produced repeatable engine-out PM emissions. The high aromatics fuel produced the highest engine-out particle concentrations, approximately a factor of 2 higher than the E50 fuel. However, the average post-GPF PM emissions were not significantly different between fuels. The post-GPF emissions were more dependent on GPF loading state than engine-out PM emissions. Fuels that emitted high engine-out PM rapidly loaded the filter and increased its filtration efficiency, while the lower engine-out emitting fuels did not effectively load the filter over the test, and therefore did not benefit from increased filtration efficiency. These results show that current and future PM emission standards could be met more easily through optimized control of GPF loading state. It is not clear whether the loading state of the GPF will be a controlled parameter in regulatory testing of PM. Optimizing the GPF loading state is a complicated control strategy. However, with proper engine calibration, emissions limits are attainable irrespective of fuel type.

Acknowledgment

This material is based upon work supported by the Department of Energy, Office of Energy Efficiency and Renewable Energy (EERE), under Award Number DE-EE0007217. This report was prepared as an account of work sponsored by an agency of the United States Government. Neither the United States Government nor any agency thereof, nor any of their employees, makes any warranty, express or implied, or assumes any legal liability or responsibility for the accuracy, completeness, or usefulness of any information, apparatus, product, or process disclosed, or represents that its use would not infringe privately owned rights. Reference herein to any specific commercial product, process, or service by trade name, trademark, manufacturer, or otherwise does not necessarily constitute or imply its endorsement, recommendation, or favoring by the United States Government or any agency thereof. The views and opinions of authors expressed herein do not necessarily state or reflect those of the United States Government or any agency thereof.

Conflict of Interest

There are no conflicts of interest.

Data Availability Statement

The authors attest that all data for this study are included in the paper. Data provided by a third party listed in Acknowledgment.

References

[1] CARB, 2012, "LEV III" Amendments to the California Greenhouse Gas and Criteria Pollutant Exhaust and Evaporative Emission Standards and Test Procedures and to the On-Board Diagnostic System Requirements for Passenger Cars, Light-Duty Trucks, and Medium-Duty Vehicles, pp. 1–161.
[2] Commission Regulation (EU) No. 459/2012. Official Journal of the European Union 2012.
[3] U.S. EPA, Light-Duty Automotive Technology, Carbon Dioxide Emissions, and Fuel Economy Trends : 1975 Through 2012 Light-Duty Automotive Technology, Carbon Dioxide Emissions, and Fuel Economy Trends: 1975 Through 2012 2017:21. 10.1002/yd.31.
[4] Liang, B., Ge, Y., Tan, J., Han, X., Gao, L., Hao, L., Ye, W., and Dai, P., 2013, "Comparison of PM Emissions From a Gasoline Direct Injected (GDI) Vehicle and a Port Fuel Injected (PFI) Vehicle Measured by Electrical Low Pressure Impactor (ELPI) With Two Fuels: Gasoline and M15 Methanol Gasoline," J. Aerosol Sci., **57**, pp. 22–31.
[5] Saliba, G., Saleh, R., Zhao, Y., Presto, A. A., Lambe, A. T., Frodin, B., Sardar, S., Maldonado, H., Maddox, C., May, A. A., Drozd, G. T., Goldstein, A. H., Russell, L. M., Hagen, F., and Robinson, A. L., 2017, "Comparison of Gasoline Direct-Injection (GDI) and Port Fuel Injection (PFI) Vehicle Emissions: Emission Certification Standards, Cold-Start, Secondary Organic Aerosol Formation Potential, and Potential Climate Impacts," Environ. Sci. Technol., **51**(11), pp. 6542–6552.
[6] Chen, L., Liang, Z., Zhang, X., and Shuai, S., 2017, "Characterizing Particulate Matter Emissions From GDI and PFI Vehicles Under Transient and Cold Start Conditions," Fuel, **189**, pp. 131–140.
[7] Piock, W., Hoffmann, G., Berndorfer, A., Salemi, P., and Fusshoeller, B., 2011, "Strategies Towards Meeting Future Particulate Matter Emission Requirements in Homogeneous Gasoline Direct Injection Engines," SAE Int. J. Eng., **4**(1), pp. 1455–1468.
[8] Berndorfer, A., Breuer, S., Piock, W., and Von Bacho, P., 2013, "Diffusion Combustion Phenomena in GDI Engines Caused by Injection Process," SAE Technical Paper No. 2013-01-0261.
[9] Piock, W. F., Befrui, B., Berndorfer, A., and Hoffmann, G., 2015, "Fuel Pressure and Charge Motion Effects on GDI Engine Particulate Emissions," SAE Int. J. Eng., **8**(2), pp. 464–473.
[10] Tanaka, D., Uchida, R., Noda, T., Kolbeck, A., Henkel, S., Hardalupas, Y., Taylor, A., and Aradi, A., 2017, "Effects of Fuel Properties Associated With In-Cylinder Behavior on Particulate Number From a Direct Injection Gasoline Engine," SAE Technical Paper No. 2017-01-1002.
[11] Frenklach, M., 2002, "Reaction Mechanism of Soot Formation in Flames," Phys. Chem. Chem. Phys., **4**(11), pp. 2028–2037.
[12] Chan, T. W., 2015, "The Impact of Isobutanol and Ethanol on Gasoline Fuel Properties and Black Carbon Emissions From Two Light-Duty Gasoline Vehicles," SAE Technical Paper No. 2015-01-1076.
[13] Storey, J. M., Barone, T., Norman, K., and Lewis, S., 2010, "Ethanol Blend Effects on Direct Injection Spark-Ignition Gasoline Vehicle Particulate Matter Emissions," SAE Int. J. Fuels Lubr., **3**(2), pp. 650–659.
[14] Maricq, M. M., Szente, J. J., and Jahr, K., 2012, "The Impact of Ethanol Fuel Blends on PM Emissions From a Light-Duty GDI Vehicle," Aerosol Sci. Technol., **46**(5), pp. 576–583.
[15] Szybist, J. P., Youngquist, A. D., Barone, T. L., Storey, J. M., Moore, W. R., Foster, M., and Confer, K., 2011, "Ethanol Blends and Engine Operating Strategy Effects on Light-Duty Spark-Ignition Engine Particle Emissions," Energy Fuels, **25**(11), pp. 4977–4985.
[16] Bock, N., Jeon, J., Kittelson, D., and Northrop, W., 2019, "Effects of Fuel Properties on Particle Number and Particle Mass Emissions From Lean and Stoichiometric Gasoline Direct Injection Engine Operation," SAE Technical Paper No. 2019-01-1183.
[17] Aikawa, K., Sakurai, T., and Jetter, J. J., 2010, "Development of a Predictive Model for Gasoline Vehicle Particulate Matter Emissions," SAE Int. J. Fuels Lubr., **3**(2), pp. 610–622.

[18] Yoshioka, F., Kato, K., Aoki, T., Makino, M., Waters, D., and Jahnke, H., 2019, "Performance of Next Generation Gasoline Particulate Filter Materials Under RDE Conditions," SAE Technical Paper No. 2019-01-0980.
[19] Miao, S., Luo, L., Liu, Y., and Zhan, Z., 2017, "Development of a Gasoline Particulate Filter for China 6(b) Emission Standards," SAE Technical Paper No. 2017-24-0135.
[20] Kęder, M., Grzeszczyk, R., Merkisz, J., Fuć, P., and Lijewski, P., 2014, "Design of a New Engine Dynamometer Test Stand for Driving Cycle Simulation," J. KONES Powertrain. Transp., **21**(4), pp. 217–224.
[21] Androne, C.-F., and Rao, S. B., 2017, *Vehicle Simulation for Powertrain System Testing*, Chalmers University of Technology, Gothenburg, Sweden.
[22] Swanson, J., and Kittelson, D., 2010, "Evaluation of Thermal Denuder and Catalytic Stripper Methods for Solid Particle Measurements," J. Aerosol. Sci., **41**(12), pp. 1113–1122.
[23] Bock, N., Jeon, J., Kittelson, D., and Northrop, W. F., 2018, "Solid Particle Number and Mass Emissions From Lean and Stoichiometric Gasoline Direct Injection Engine Operation," SAE Technical Paper No. 2018-01-0359.
[24] Maricq, M. M., and Xu, N., 2004, "The Effective Density and Fractal Dimension of Soot Particles From Premixed Flames and Motor Vehicle Exhaust," J. Aerosol. Sci., **35**(10), pp. 1251–1274.
[25] Terres, A., Ebert, V., Nowak, A., Rosahl, J., Hildebrandt, M., Southgate, J., Usarek, S., Cresnoverh, M., Marshall, I., Mamakos, A., Giechaskiel, B., Bacher, H., Horn, H., and Kaatz, M., 2018, Particle Measurement Programme (PMP): Inter-Laboratory Correlation Exercise With Condensation Particle Counters (CPCs). 10.2760/859241.
[26] Hinds, W. C., 1999, *Aerosol Technology: Properties, Behaviour, and Measurement of Airborne Particles*, 2nd ed., Wiley-Interscience, New York.